ChemComm

COMMUNICATION

View Article Online
View Journal

Cite this: DOI: 10.1039/d6cc00921b

Received 11th February 2026,
Accepted 2nd April 2026

DOI: 10.1039/d6cc00921b

rsc.li/chemcomm

A nanoporous hygroscopic pectin-based sorbent for atmospheric water harvesting

Sonali Seth,[a] Ankit Nagar,[a] Tanmayaa Nayak,[a] Vivek Yadav,[a] Sujan Manna[a] and Thalappil Pradeep *[ab]

A porous hygroscopic biopolymeric sorbent (PTPA) composed of biocompatible polysaccharide pectate (PT) functionalised with polyacrylic acid (PA) was developed, exhibiting enhanced water uptake of 3.8 g g^{-1} at 99% RH and efficient release. The synergistic molecular structure and functional groups of the PTPA enable humidity capture, high storage capacity, rapid vapor release and efficient regeneration within 120 min upon exposure to 1 kW m^{-2} solar simulator irradiation.

Freshwater scarcity is an escalating global challenge, with India projected to be among the most severely affected nations by 2050, hosting the world's largest population under water stress.[1] Atmospheric water harvesting (AWH) offers great potential to mitigate this crisis, as the earth's atmosphere contains approximately 1.42×10^{19} litres of freshwater, equivalent to nearly 1.8 billion litres per person.[2] Among various approaches, sorption-based AWH (SAWH) is one of the viable, cost- and energy-efficient methods for decentralised freshwater production, being independent of geographical and hydrological constraints. In SAWH, a hygroscopic, porous adsorbent captures moisture from the air, and the adsorbed water is released as vapors through mild heating, such as solar energy.[3] The released vapours can be trapped and converted to liquid water by placing the sorbent in a closed chamber such that the vapor condenses to liquid, enabling decentralised water production.[4] Recent studies have shown the integration of adsorbents with solar-driven AWH systems.[5] Conventional hygroscopic sorbents often face limitations such as high cost, agglomeration, and contamination of the produced water.[6] To overcome these issues, polymeric hydrogels have emerged as promising next-generation sorbents due to their cross-linked porous networks enriched with abundant hydrophilic sites (–OH, –COOH, $–SO_3H$), which facilitate efficient water capture through hydrogen bonding and electrostatic interactions.[7,8] In this context, studies from Guo *et al.* have highlighted the importance of precisely manipulating polymeric chain interactions to enhance water retention, mechanical properties and mass transport in hydrogels.[9] Also, the thermal stability and the robustness of the sorbent in water play a major role.[10,11] However, challenges related to the limited understanding of polymer–water interactions governing sorption behaviour still persist. To address these challenges and gain deeper insights into understanding the role of active functionalities, this study explored the role of sorbent design for enhanced moisture sorption and release.

Herein, pectin (PC), a biocompatible and inexpensive polymer with excellent gelling properties, was chosen as the polymeric support.[12] To enhance its water sorption capacity and thermal stability, PC was converted to PT and subsequently functionalized with acrylic acid (AA) *via* free radical polymerisation, using *N*,*N*′-methylenebisacrylamide (MBA) as a cross-linker. The resulting sorbent (PTPA) exhibited a high-moisture uptake of 3.8 g g^{-1} at 99% RH within 48 h without the incorporation of hygroscopic salts and demonstrated remarkable stability over repeated sorption–desorption cycles (Fig. 1a).

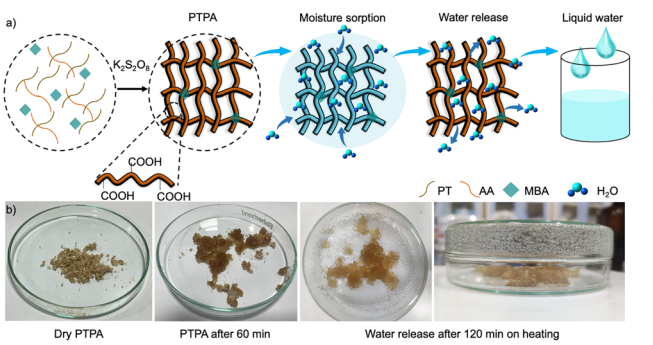

Fig. 1 a) Schematic for the synthesis of PTPA for SAWH. (b) Photographs of PTPA covered by the Petri dish, at various time intervals.

[a] DST Unit of Nanoscience (DST UNS) and Thematic Unit of Excellence (TUE), Department of Chemistry, Indian Institute of Technology Madras, Chennai 600036, India. E-mail: pradeep@iitm.ac.in

[b] International Centre for Clean Water, IIT Madras Research Park, Chennai 600113, India

Vibrational spectroscopic analyses (FTIR and Raman) were conducted to elucidate the site-specific molecular interactions governing moisture capture in PTPA. Owing to its hierarchical and interconnected structure, PTPA absorbs water vapors that diffuse into the polymeric network and is retained through active functional groups. Upon heating the bottom of Petri dish at 50 °C the released vapors condensed on the walls of the Petri dish as macroscopic droplets, which could then be collected as shown in Fig. 1b.

In this work, PC was first converted to PT (details in the SI). FTIR analysis confirmed the de-esterification of PC to PT, as evidenced by the disappearance of the ester carbonyl peak at 1734 cm^{-1} (–$COOCH_3$) and the appearance of a strong band at 1589 cm^{-1} (asymmetric stretch of COO^-) (Fig. S1).[13,14] AA was polymerised to PA, where the disappearance of the peak at 1630 cm^{-1} (C=C stretch) and the appearance of a new peak at 1552 cm^{-1} (amide-II stretch) confirmed the incorporation of MBA and formation of cross-linked PA (Fig. S2).[15] Subsequently, PC and PT were functionalised with AA under identical reaction conditions. For PCPA, characteristic peaks at 1716 cm^{-1} (–C=O stretching), 1548 cm^{-1} (amide-II), 1403 cm^{-1} (symmetric –COO^- stretching), and a broad overlapped region from 1100–1000 cm^{-1} (–C–O and –O–H stretching) confirmed the grafting of PC to PA (Fig. S3).[16,17] In contrast, the FTIR spectrum of PTPA (Fig. 2a) showed an additional intense band at 1634 cm^{-1}, attributed to the overlap of amide-I and asymmetric COO^- stretch, indicating the grafting of PT to PA, forming PTPA and incorporation of additional active sites within the polymeric network (Fig. S4).[18,19] The microstructural features of the sorbents play a crucial role in enhancing moisture capture, facilitating vapor transport, and ensuring long-term stability.[20–22] Microscopic analysis revealed that PTPA exhibit a hierarchical, petal-like porous morphology, distinct from PC, PA and PCPA (Fig. 2b–d and Fig. S5). In the case of PTPA, an interconnected porous network was developed that promoted efficient vapor transport, while its exposed active sites facilitated enhanced moisture capture and storage, unlike PC and PA, where the surfaces were relatively smooth and lacked well-developed pores. Although PA is inherently hygroscopic, it did not exhibit sufficient capacity for enhanced moisture capture due to the absence of a hierarchical structure. While PCPA showed a rougher surface, the active sites were not adequately exposed to achieve effective water sorption. It is worth noting that in the case of PTPA, the abundant –COO^- sites of PT served as anchoring sites for growth of PA chains, resulting in a cross-linked hierarchical network in which the –COO^- groups from both PT and PA remained exposed on the surface, enhancing water sorption and storage, while MBA remained embedded within the polymeric network, contributing to structural integrity without affecting the active sites.

The thermal stability profiles of PC, PA, PCPA and PTPA (Fig. S6) reveal that all sorbents show a three-step thermal degradation pattern. Among them, PC showed the poorest stability with early decomposition due to its water loss, followed by the breakdown of polysaccharide chains.[23] PA demonstrated moderately improved stability but experienced rapid degradation around 400 °C due to decarboxylation and decomposition associated with its –COOH groups.[24] In comparison, PTPA degraded more slowly than PCPA, owing to its stronger cross-linked polymeric network. Furthermore, the abundant –COO^- and –COOH groups in PT provided more interaction sites, facilitating stronger hydrogen bonding, improved inter- and intra-molecular interactions, and a denser gel structure, which contributed to the superior thermal stability of PTPA.[25]

To evaluate the sorbent's moisture uptake performance, the dried sorbents were exposed to humid air (99% RH, 25 °C), and their uptake capacities were compared (Fig. 3a). The grafting of PT to AA enhanced the moisture uptake to 3.8 g g^{-1}, compared to PC, PA and PCPA, due to its abundant –COO^- and –COOH functional groups in PTPA together with its hierarchical petal-like structure that facilitated vapour diffusion and sorption. PC showed the lowest moisture uptake because of limited hydrophilic functionalities, being dominated by –$COOCH_3$ groups. The PTPA was further evaluated under different humid conditions (10% RH-99% RH, 25 °C), and it demonstrated 0.3,

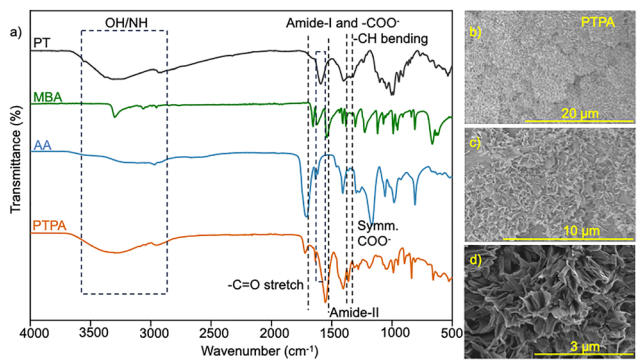

Fig. 2 (a) FTIR spectra for the functionalisation of PT to PA using MBA as the cross-linker, *via* free radical polymerisation. (b) FESEM image of PTPA (20 μm). (c) and (d) Magnified view of PTPA (10 μm, 3 μm).

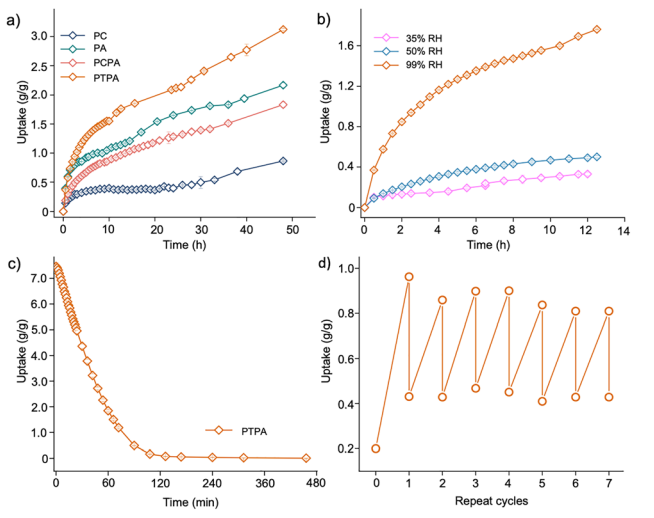

Fig. 3 (a) Moisture uptake kinetics of PC, PA, PCPA and PTPA at 99% RH and 25 °C. (b) Moisture uptake kinetics of PTPA at 25 °C and different humidity levels. (c) Desorption kinetics of PTPA under 1 Sun illumination. (d) Cyclic stability of PTPA for moisture sorption and desorption.

0.49 and 1.69 g g^{-1} water uptake at 35, 50, 99% RH, respectively within 12 h, without the presence of hygroscopic salts (Fig. 3b). The high-performance and salt-free sorbent's hygroscopic properties highlight its reliability and practical potential in SAWH. To understand the sorption behaviour of PTPA and the role of active sites, the moisture uptake of PTPA was measured over a range of relative humidity levels from 5% to 95% using a dynamic vapor sorption analyzer. As shown in Fig. S7, PTPA exhibited Type III sorption isotherm, and the surface area of PTPA came out to be 190 m^2 g^{-1}.

Efficient desorption of captured vapors plays a critical role in achieving efficient SAWH performance. As shown in Fig. 3c, Saturated PTPA released the captured moisture completely within 120 min under simulated solar irradiation (1 kW m^{-2}), demonstrating its rapid and enhanced water release capacity. This fast release is attributed to its interconnected porous network.[26] Thermal imaging under 1 Sun further confirmed its photothermal conversion capability, with the surface temperature of PTPA reaching 51 °C within 120 min (Fig. S8), sufficient to weaken hydrogen bonds and accelerate the water release.

The cyclic stability of PTPA was investigated through repeated adsorption–desorption cycles (Fig. 3d). In the first cycle, the sorbent was exposed to 99% RH for 60 min, followed by 60 min of solar irradiation (1 kW m^{-2}) for desorption. From the second cycle onward, the adsorption time was reduced to 30 min, followed by a 45-min desorption period. PTPA maintained stable performance over seven consecutive cycles. In all cycles except the first, the sorbent achieved 100% desorption of the adsorbed moisture, attributed to the strong hygroscopic nature of PTPA. In the first cycle, complete desorption was not achieved within the allotted time due to the higher initial moisture uptake; however, extended exposure to solar irradiation enabled complete moisture release within 120 min. This behaviour is consistent with recent studies where strong polymer–water interactions in hygroscopic gels lead to locked water within the network.[27,28] To identify the stability of PTPA under natural conditions, PTPA was exposed to normal laboratory conditions for 1 month, and FTIR showed no noticeable changes compared to the original material, indicating that the composite remained structurally stable (Fig. S9) and did not undergo microbial degradation under these environmental conditions. Also, PTPA was exposed to 99% RH for 7 days, and we observed leakage on the 7th day, indicating its long-term stability and high swelling capacity (Fig. S10). The leakage was due to the saturation of active sites. The future work will focus on improving water retention through modifying the composite design, including the incorporation of inorganic components like FeOOH.[29]

To identify the active sites involved in moisture capture, time-dependent ATR-IR measurements were performed by exposing PTPA to 99% RH, starting from 30 min to 240 min. The corresponding parent IR spectra are in Fig. S11, and the deconvoluted region (2000–1000 cm^{-1}), focusing on the relevant features, is shown in Fig. 4. Peak shift from 1716 to 1692 cm^{-1} (–C═O stretch) along with the red shift of COO^-

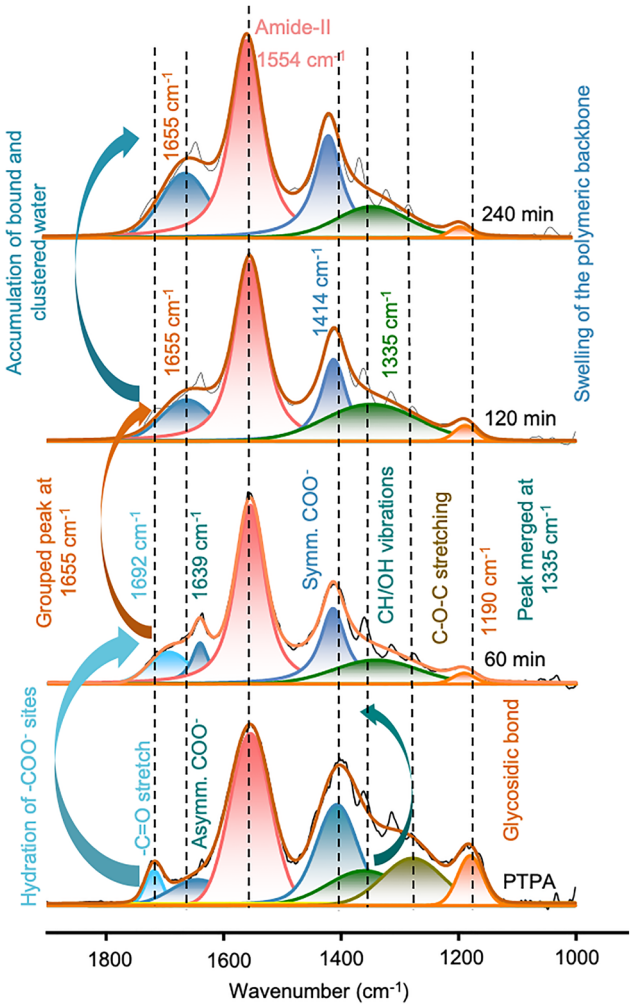

Fig. 4 Deconvoluted time-dependent IR spectra of PTPA at regular time intervals after exposure to 99% RH. The composite spectra are shown as thick lines. The experimental spectra are shown as thin lines. Individual C–O–/C–H/–OH peaks at 1310 cm^{-1}, C–O–C at 1360 cm^{-1}, and COO^- at 1710 cm^{-1} were not fitted separately. Chamber was maintained at 99% RH.

groups (1620 to 1639 cm^{-1} and 1405 to 1414 cm^{-1}) indicated hydration of $–COO^-$ sites within 60 min, suggesting $–COO^-$ sites as the primary active sites for moisture absorption. Additionally, a peak shift in the glycosidic backbone of PTPA, from 1178 cm^{-1} to 1190 cm^{-1} after 60 min, suggested hydration of the polymeric chain, beyond which no further change was observed. The fitted peaks centred at 1352 cm^{-1} (–CH/–OH vibrations)[28,30] and 1274 cm^{-1} (C–O–C stretching) were observed in the case of PTPA because of grouped vibrational modes.[16] Upon prolonged exposure at 99% RH, these peaks merged into a broader peak at 1335 cm^{-1}, arising from grouped frequencies of C–O–/C–H/–OH functionalities, along with the contribution from adsorbed water,[31] suggesting backbone swelling and hydration, where water vapor diffused and disrupted intra-polymer hydrogen bonds. In contrast, no peak change at 1554 cm^{-1} (amide-II)[32] was observed in 240 min, indicating its minimal involvement in moisture capture. A broad peak centred at 1655 cm^{-1} (coupled vibration of–COO^- and H_2O

bending)[33] appeared after 60 min and intensified within 240 min, signifying the accumulation of bound and clustered water within the polymeric network.

To investigate the state of adsorbed water in PTPA during vapor sorption, Raman spectroscopy was performed after 240 min of exposure at 99% RH. A broad –OH stretching band (3200–3800cm^{-1}) centred at 3497.5 cm^{-1} was observed (Fig. S12). Deconvolution of this region revealed five distinct peaks. The peaks at 3373 and 3444.4 cm^{-1} are associated with symmetric and asymmetric tetrahedral structures of free water.[34] The bands at 3510 cm^{-1} and 3568 cm^{-1} represent intermediate water involved in partially disrupted hydrogen bonding and non-tetrahedral structures within PTPA,[34] whereas the peak at 3635 cm^{-1} is for weakly bound or free water, enabling low-energy evaporation.[35,36]

To enable the development of practical SAWH systems for decentralized access to clean water, it is essential to evaluate the cost of the developed sorbent. The cost of PTPA was compared with that of existing SAWH sorbents (Table S1).[37] PTPA was found to be comparatively inexpensive, with a material cost of \$ 0.027 g^{-1} for 1 kg of water production per day, which is lower than that of most reported materials. Furthermore, the synthesis does not involve the use of organic solvents, making the process greener and reducing material wastage, thereby enhancing the feasibility and practical potential of PTPA for large-scale and decentralized SAWH applications.

In this work, SAWH sorbent was developed without the use of hygroscopic salts, demonstrating efficient moisture capture and release along with repeated cyclic stability. The interconnected petal-like hierarchical structure enables the moisture capture, while the active sites of PTPA promote the hydration and storage of water molecules within the network, as confirmed by the time-dependent FTIR studies. Overall, this work presents a cost-effective sorbent for SAWH, improving the feasibility and affordability.

Conflicts of interest

There are no conflicts to declare.

Data availability

The data supporting this article are included in the main article and its supplementary information (SI). Supplementary information is available. See DOI: https://doi.org/10.1039/d6cc00921b.

No additional data has been deposited in external repositories.

Acknowledgements

The authors thank the Sophisticated Analytical Instrumentation Facility (SAIF), IIT Madras, for TGA measurements, and the Department of Chemistry, IIT Madras, for providing certain research facilities. T. P. acknowledges financial support from SERB-SUPRA (Grant No. SPR/2021/000439), and the Centre of Excellence on Molecular Materials and Functions under the Institution of Eminence scheme of IIT Madras. S. S. and V. Y. thank the Ministry of Education for their Prime Minister's Research Fellowship. The authors also thank the Department of Science and Technology, Government of India, for supporting the research program on nanomaterials and Prof. Aravind Kumar Chandiran, Department of Chemical Engineering, IIT Madras, for providing access to the solar simulator and infrared camera for the experiments. We also thank Prof. Manu Jaiswal for allowing access to the dynamic vapor sorption analyser.

References

1 C. He, Z. Liu, J. Wu, X. Pan, Z. Fang, J. Li and B. A. Bryan, *Nat. Commun.*, 2021, **12**, 4667.
2 A. Nagar and T. Pradeep, *ACS Nano*, 2020, **14**, 6420–6435.
3 H. Shan, P. Poredoš, Z. Chen, X. Yang, Z. Ye, Z. Hu, R. Wang and S. C. Tan, *Nat. Rev. Mater.*, 2024, **9**, 699–721.
4 M. Ejeian and R. Z. Wang, *Joule*, 2021, **5**, 1678–1703.
5 S. Guo, Y. Zhang and S. C. Tan, *Device*, 2023, **1**, 100099.
6 Y. Guo, W. Guan, C. Lei, H. Lu, W. Shi and G. Yu, *Nat. Commun.*, 2022, **13**, 2761.
7 S. Loo, L. Vásquez, A. Athanassiou and D. Fragouli, *Adv. Mater. Interfaces*, 2021, **8**, 2100580.
8 Y. Guo, J. Bae, Z. Fang, P. Li, F. Zhao and G. Yu, *Chem. Rev.*, 2020, **120**, 7642–7707.
9 S. Guo, S. Zhang, H. Li, S. Liu, J. J. Koh, M. Zhou, Z. Sun, Y. Liu, H. Qu, Z. Yu, Y. Zhang, L. Yang, W. Chen, C. He, C. Lee, D. Mao, S. K. Ravi, Y. Lai and S. C. Tan, *Matter*, 2025, **8**, 101785.
10 V. Yadav, A. Jana, S. Acharya, S. Malola, H. Nagar, A. Sharma, A. R. Kini, S. Antharjanam, J. Machacek, K. N. V. D. Adarsh, T. Base, H. Häkkinen and T. Pradeep, *Nat. Commun.*, 2025, **16**, 1197.
11 S. Zhang, J. Fu, G. Xing, W. Zhu and T. Ben, *ChemistryOpen*, 2023, **12**, e202300046.
12 S. Huang, Y. Zhang, Q. Chen, Y. Liu, L. Lu, M. M. Arain, Z. Li, S. Pan and F. Liu, *Food Hydrocoll.*, 2025, **160**, 110841.
13 M. A. Monsoor, U. Kalapathy and A. Proctor, *J. Agric. Food Chem.*, 2001, **49**, 2756–2760.
14 Z. Zhao, Y. Hwang, Y. Yang, T. Fan, J. Song, S. Suresh and N.-J. Cho, *Proc. Natl. Acad. Sci. U. S. A.*, 2020, **117**, 8711–8718.
15 J. Zhang, D. Qu, S. Wang, S. Qi and H. Zuo, *Polymers*, 2024, **16**, 1990.
16 G. Kowalski, K. Kijowska, M. Witczak, Ł. Kuterasiński and M. Łukasiewicz, *Polymers*, 2019, **11**, 114.
17 M. Karmakar, H. Mondal, M. Mahapatra, P. K. Chattopadhyay, S. Chatterjee and N. R. Singha, *Carbohydr. Polym.*, 2019, **206**, 778–791.
18 W. Jia, M. Li, L. Kang, G. Gu, Z. Guo and Z. Chen, *J. Mater. Sci.*, 2019, **54**, 10871–10883.
19 K. Saito, T. Xu and H. Ishikita, *J. Phys. Chem. B*, 2022, **126**, 4999–5006.
20 L. Liu, W. Li, X. Wang, X. Wang, G. Ma, L. Zhu and Y. Xu, *Chem. Commun.*, 2025, **61**, 16826–16829.
21 D. Sarkar, A. Mahapatra, A. Som, R. Kumar, A. Nagar, A. Baidya and T. Pradeep, *Adv. Mater. Interfaces*, 2018, **5**, 1800667.
22 A. Nagar, R. Kumar, P. Srikrishnarka, T. Thomas and T. Pradeep, *ACS Appl. Nano Mater.*, 2021, **4**, 1540–1550.
23 K. M. Wani and R. V. S. Uppaluri, *Appl. Food Res.*, 2023, **3**, 100345.
24 M. A. Moharram and M. G. Khafagi, *J. Appl. Polym. Sci.*, 2006, **102**, 4049–4057.
25 M. M. Fares, Y. R. Tahboub, S. T. Khatatbeh and Y. M. Abul-Haija, *J. Polym. Environ.*, 2011, **19**, 431–439.
26 K. Nabeela, M. N. Thorat, S. N. Backer, A. M. Ramachandran, R. T. Thomas, G. Preethikumar, A. P. Mohamed, A. Asok, S. G. Dastager and S. Pillai, *ACS Appl. Bio Mater.*, 2021, **4**, 4373–4383.
27 S. Guo, Y. Zhang, Z. Yu, M. Dai, X. Liu, H. Wang, S. Liu, J. J. Koh, W. Sun, Y. Feng, Y. Chen, L. Yang, P. Sun, G. Lu, C. Yu, W. Chen, S. De Wolf, Z. Wang and S. C. Tan, *Nat. Commun.*, 2025, **16**, 5267.
28 S. Guo, S. Patel, J. Wang, Z. Yu, H. Qu, S. Zhang, K. Yu, S. Liu, J. J. Koh, X. Q. Koh, Z.-E. Ooi, D. H. L. Seng, W. Sun, L. Yang,

Y. Zhang, J. Wang, S. K. Ravi, C. Yu and S. C. Tan, *Sci. Adv.*, 2025, **11**, eadw5991.
29 A. A. Kumar, A. Som, P. Longo, C. Sudhakar, R. G. Bhuin, S. S. Gupta, Anshup, M. U. Sankar, A. Chaudhary, R. Kumar and T. Pradeep, *Adv. Mater.*, 2017, **29**, 1604260.
30 T. Nayak, S. Mukherjee, A. R. Kini, M. R. Islam, A. Nagar, S. Seth and T. Pradeep, *ACS Sustainable Chem. Eng.*, 2025, **13**, 1838–1850.
31 S. A. Iyengar, P. Srikrishnarka, S. K. Jana, M. R. Islam, T. Ahuja, J. S. Mohanty and T. Pradeep, *ACS Appl. Electron. Mater.*, 2019, **1**, 951–960.
32 S. Seth, M. R. Islam, T. Nayak, A. R. Kini, S. Manna, B. K. Malla, A. Nagar and T. Pradeep, *ACS Sustainable Chem. Eng.*, 2025, **13**, 10918–10929.
33 A. Barth, *Biochim. Biophys. Acta, Bioenerg.*, 2007, **1767**, 1073–1101.
34 F. Li, N. Li, S. Wang, L. Qiao, L. Yu, P. Murto and X. Xu, *Adv. Funct. Mater.*, 2021, **31**, 2104464.
35 S. Kim, Y. Liang, S. Kang and H. Choi, *Chem. Eng. J.*, 2021, **425**, 131601.
36 Q. Sun, *Vib. Spectrosc.*, 2009, **51**, 213–217.
37 F. Deng, C. Wang, C. Xiang and R. Wang, *Nano Energy*, 2021, **90**, 106642.